Corrosion Science 130 (2018) 218–230

Contents lists available at ScienceDirect

Corrosion Science

journal homepage: www.elsevier.com/locate/corsci

Localized corrosion behaviour of AA7150 after ultrasonic shot peening: Corrosion depth vs. impact energy

Qingqing Sun[a,b], Qingyou Han[a,*], Rong Xu[c], Kejie Zhao[c], Jie Li[b]

[a] School of Engineering Technology, Purdue University, West Lafayette, IN 47907, United States
[b] School of Chemistry and Chemical Engineering, Central South University, Changsha, Hunan 410012, China
[c] School of Mechanical Engineering, Purdue University, West Lafayette, IN 47907, United States

ARTICLE INFO

Keywords:
AA7150
Surface nanocrystallization
Localized corrosion
Impact energy
Kinetics

ABSTRACT

The effect of impact energy on localized corrosion behaviour of ultrasonic shot peened AA 7150 was systematically studied by manipulating peening parameters such as peening duration, peening amplitude, peening distance and peening media size. Needle-like pits with depths deeper than that of the untreated alloy were observed on low energy peened samples. However, localized corrosion was eliminated for high energy peened alloys. The formation of equiaxed nanograins on surface layer significantly enhanced pit initiation resistance but accelerated propagation kinetics. Galvanic interaction between surface layer and substrate alloy caused by surface segregation was also discussed.

1. Introduction

Surface mechanical attrition treatment (SMAT) is a technique to induce strain hardening and nanocrystallization of the surface of alloys through applying severe plastic deformation (SPD) [1,2]. Ultrasonic shot peening (USSP) is a novel method of SMAT to achieve surface SPD [3,4]. Through "playing with defects" [5], SMAT/USSP simplifies the overall composition of high performance metals. The alloys are less dependent on elements in short supply and more easily recoverable at the end of life. In addition, alloys can avoid disadvantages, such as poor ductility properties, when processed with bulk SPD techniques [6]. Thus, SMAT is a very promising technique for future alloy application. SMAT is an effective strategy for enhancement in fatigue resistance [7], reduction of friction coefficient and wear rates [8], lowering nitriding temperature [2] and increasing diffusion rate [9].

From a sustainability viewpoint, corrosion properties of SMATed materials also should be taken into account. The investigation of the corrosion mechanism of the SMATed alloy may provide a better understanding of other surface performances such as fatigue because corrosion and other surface/interface properties are usually mutually related. A significant body of research exists regarding the effect of SMAT/USSP on the corrosion performance of alloys [10–24]. Both beneficial and deleterious effects caused by SMAT/USSP have been reported. Uroš Trdan el.al [25] reported that after laser shot peening, AA6082-T651 showed an enhanced passivity with corrosion current reduction by as much as a factor of 12 compared to the untreated specimen. XPS analysis indicated Al_2O_3 enrichment accounts for the enhancement in corrosion. However, there was a significant body of research reported that SMAT results in a deleterious influence on corrosion performance of Al alloys [12–14,23,26]. Mustafa Abdulstaar et al. [12] compared bulk and surface severe plastic deformation in relation to the corrosion behaviour of AA5083. The bulk SPD was performed through rotary swaging. The surface-induced SPD was conducted by applying shot peening and ball burnishing. Results revealed that better corrosion resistance was achieved after bulk SPD. However, both shot peening and ball burnishing led to deterioration in corrosion resistance. Likewise, R.A. Waikar et al. [13] conducted air blast shot peening (ABSP) on two types of Al alloy viz. AA6061 and AA7075. The results found that the corrosion rates of these ABSP samples are higher than their bulk counterparts as revealed by electrochemical tests performed in a simulated body fluid (Hank's solution).

Impact parameters such as peening media diameter and duration influence the corrosion performance of SMATed alloys. Pandey et al. [27] investigated the effects of ultrasonic shot peening duration on corrosion performance of AA 7075. The sample USSPed for 15 s, 30 s and 60 s exhibited lower current density as compared with that of the untreated specimen. But for the USSPed 300 s sample, the current density was higher than that of the untreated. Balusamy et al. [28] studied the influence of SMAT parameters on corrosion behaviour of AISI 409 grade stainless steel in 0.6 M NaCl using electrochemical methods. Using 2 mm Ø 316L stainless steel (SS) balls for 15, 30 and 45 min and 5 mm Ø balls for 15 min offered a better corrosion

* Corresponding author.
E-mail address: hanq@purdue.edu (Q. Han).

https://doi.org/10.1016/j.corsci.2017.11.008
Received 11 July 2017; Received in revised form 4 November 2017; Accepted 8 November 2017
Available online 10 November 2017
0010-938X/

protective ability. In contrast, treatments using 5 mm Ø balls for 30 and 45 min and 8 mm Ø balls for 15, 30 and 45 min increased corrosion rate due to the introduction of microstrain and higher density defects. The results [27,28] indicate that high energy SMAT leads to a deleterious effect while low energy SMAT leads to a beneficial effect on corrosion behaviour.

However, the previously discussed phenomenon is absent for 304 SS [19]. Treatments using 2, 5 and 8 mm Ø balls for 900, 1800, 2700 and 3600 s all result in a deleterious influence. The extent of corrosion attack on 304 SS surface is more severe for samples treated using 5 and 8 mm Ø balls than those treated using 2 mm Ø balls. Corrosion depth was not measured and compared by Balusamy's group [19,28], so the localized corrosion resistance maybe different with electrochemical results. Gupta et al. [29] reported that multiple layer peening effectively suppresses intergranular corrosion (IGC) susceptibility of SS304. The suppression was due to the breakage of the intergranular network of chromium carbide-/chromium-depleted regions under the influence of high rate plastic deformation imposed by multiple peening treatment. Unlike the contradictory results in corrosion rate obtained using electrochemical methods, the improved IGC results of SMAT obtained by different researchers [29–32] showed a very good consistency.

The authors of the current paper believe the inconsistent electrochemical data is mainly caused by the surface contamination that resulted from shot media and/or USSP setup enclosure [23,33–37]. In a recent work [4], the surface contamination layer mainly containing Fe and Ti has been proven to account for the significant increment of corrosion rate of AA 7150 subjected to high impact energy USSP. After the exfoliation of contamination layer, corrosion rate of USSP treated samples turn out to be lower than that of the controlled sample.

The effect of SMAT on corrosion varies with alloy system [15,16,19,20], grain orientation [10], corrosive environment [21], temperature [22], impact medium [23,24] and etc. Systematic understanding of corrosion behaviour for surface nanocrystallized materials is currently lacking however [6]. Two critical aspects have been ignored in this area. The first one is the localized corrosion nature of alloys. For example, for 2000 and 7000 series ultra-high strength Al alloys, localized corrosion such as pitting and IGC is more common and detrimental than uniform corrosion. Unfortunately, most published work only studied corrosion rate using electrochemical methods [12–24] while only several works included the measured corrosion depth in their work [10,11].

Ye et al. [11] obtained cross-sectional morphologies of AA7085 alloy with and without shot peening after IGC tests. The work found that the average IGC depth reduced from 176.4 μm to 61.5 μm after shot peening. Liu and Frankel [10] studied the effect of low plastic burnishing (LPB) on IGC of AA2024-T3 alloy. LPB can induce the compressive layer with a depth of 1 mm and significantly increase the breakdown potential, as revealed by a micro-capillary cell technique. The change of IGC depth of alloys before and after LPB treatment depends on surface orientation with respect to rolling direction. For L direction, the depths of attack before and after LPB treatment are similar. For the S direction, the mean depth of attack reduced from 193 ± 31 μm to 141 ± 42 μm after LPB treatment. The localized nature of corrosion deserves more attention from researchers. To our best knowledge, the effect of peening parameters on localized corrosion depth has not been reported yet. The current work is the first to reveal the relationship between gradient microstructure and localized corrosion kinetics of alloy subjected to SMAT/USSP.

Another frequently ignored aspect is the galvanic interaction. After SPD processing and especially after surface SPD treatment, the potential of a newly formed layer of alloy changed. The change in potential was due to element segregation [4], grain refinement [1,2,38], elements redistribution [39], change of passive oxide film [22] and foreign impurities induced [24]. The potential difference between nanocrystalline surface layer and the interior will result in an electron transfer and galvanic corrosion. Therefore, the current work investigated the effects of USSP parameters such as peening duration, peening amplitude, peening distance and peening media diameter on localized corrosion along with the galvanic corrosion of AA7150. Kinetics of localized corrosion initiation and propagation of alloys after surface nanocrystallization was summarized. The relationship between microstructure, surface composition, galvanic interaction and localized corrosion kinetics was established.

Table 1
Chemical composition of AA 7150 (mass fraction, *wt.*%).

Zn	Mg	Cu	Mn	Si	Fe	Cr	Zr	Ti	V	others	Al
6.5	2.3	2.3	0.1	0.12	0.15	0.04	0.10	0.06	0.00	0.15	Rem.

2. Experimental

2.1. Materials

The material used in this work is a commercially available 7150 aluminium alloy rolled plate received from Alcoa Corp. and treated with the T7751 aging process. Alloy was cut into specimens with thickness of 6 mm and the dimension of 50 × 50 mm^2, then grinded using #400 sand paper before USSP treatment. The composition (in mass fraction) is listed in Table 1. The 3D optical microstructure of the rolled AA 7150 etched by Keller' reagent is shown in Fig. 1.

2.2. USSP setup and peening parameters

Fig. 2 shows the schematic diagram of USSP setup [40]. AA 7150 specimens were fixed using a cylindrical enclosure made by cast iron with inner diameter of 25 mm. USSP was applied on the ND plane of the alloy. Powered by a VCF-1500 ultrasonic processor (Sonic & Materials, Newtown, CT) with the frequency of 20 kHz, the S440 stainless steel balls with different diameters were used as shot peening media. During ultrasonic shot peening, the top surface of the horn was covered with a layer of shots.

A given USSPed sample can be characterized with four different parameters:

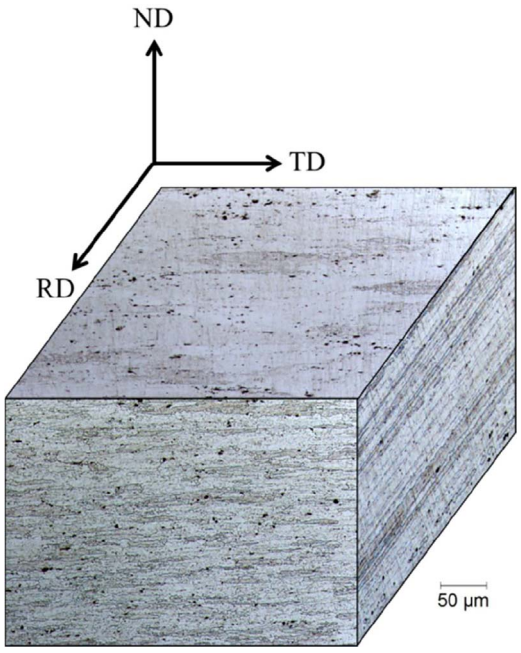

Fig. 1. 3D optical microstructure of AA 7150.

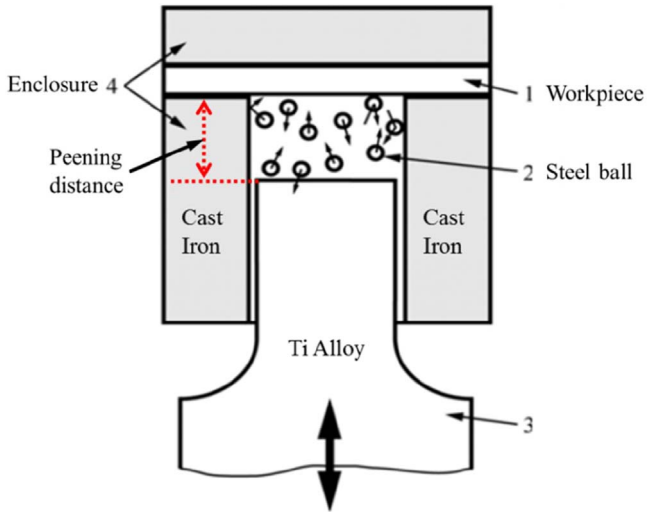

Fig. 2. Ultrasonic shot peening setup consists of (1) work piece, (2) stainless steel shots, (3) horn which is connected to a transducer and generator of ultrasonic signals, and (4) enclosure.

D-d-A-t

where, *D* is the diameter of stainless steel ball. *d* is the peening distance which represents the distance between the top surface of the horn and the bottom surface of specimens. *A*, amplitude, measured in microns, is the peak to peak, up and down distance (excursion) that the probe tip travels. The higher the amplitude set point, the greater the amount of energy that will be transmitted onto the alloy surface. The amplitude at the probe tip depends on the diameter of the probe and the amplitude selected using the Output Control. In the current work, the 25 mm Ø probe had an excursion (travel) of 70 μm when $A = 100\%$ of Output Control. Because the Output Control circuitry is linear, the same probe will have an excursion (travel) of 35 μm when $A = 50\%$. And finally, *t* is the peening duration.

We can manipulate these four different parameters to tune the impact energies applied on specimens. Table 2 exhibits the four groups of experimental parameters.

2.3. Localized corrosion depth

According to ASTM standard G110-92, 57 g/L NaCl + 10 mL/L H_2O_2 was chosen as intergranular corrosion (IGC) solution for the measurement of corrosion depth. The exposure was conducted in a vessel holding 15 mL of test solution per square cm of specimen surface area at room temperature. The exposure duration was 24 h. After exposure, the specimens were rinsed with water. The cross-section of the exposure surface was etched with Keller' reagent. The maximum corrosion depth of more than 15 images (each image was 2.679 mm in length and corresponded to a maximum depth) was measured. Then the average value of maximum corrosion depths and the maximum depth of all the obtained images was calculated and compared for the untreated and USSPed alloys. The untreated represents specimen without peening treatment but receives the same treatment prior to USSP.

Table 2
Four groups of USSP experimental parameters (*D*, *d*, *A* and *t* means peening media diameter, peening distance, ultrasonic amplitude and peening duration, respectively. E.g. 3mm-8.2mm-80%-*t* group represents specimens treated with 3 mm Ø stainless steel ball, 8.2 mm peening distance, 80% of the full ultrasonic amplitude and various peening durations).

3mm–8.2mm–80%-*t*	7.5 s	30 s	2 min	4 min	8 min	16 min
4mm-10mm-*A*–8 min	30%	40%	60%	80%	100%	
3mm-*d*-80%–8 min	18 mm	15 mm	12 mm	9 mm	6 mm	
D-10mm-80%–8 min	1 mm	3 mm	5 mm			

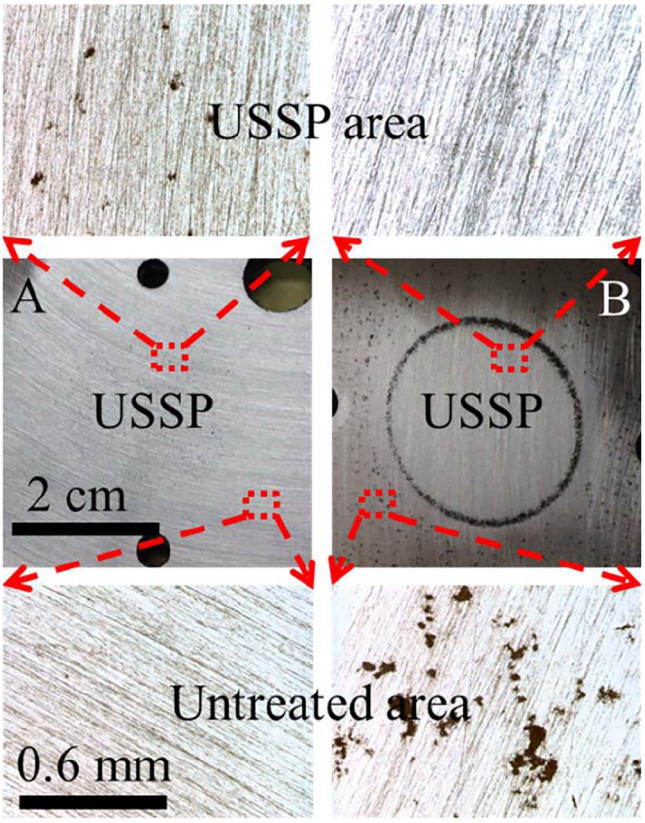

Fig. 3. A quick method used for comparing the relative corrosion depth of untreated area and USSPed area: the pits of USSPed area are deeper (sample A); the pits of untreated area are deeper (sample B). The method is carefully grinding the samples after IGC tests until the absence of pits on either USSPed area or untreated area.

An effective method for comparing the relative corrosion depth of untreated and USSPed alloys was achieved with the assistance of unaided eye/optical microscopy. The USSPed sample is a 50 × 50 mm plate with Ø 25 mm circular area that was shot peened. After carefully grinding until no pits on either the USSPed area or untreated area was seen, the relative corrosion depth could be determined. As shown in Fig. 3, pits of USSPed area are deeper for the sample A. Conversely for sample B, pits of the untreated area are deeper.

2.4. Electrochemistry

The VersaSTAT 3 potentiostat/galvanostat connected to a three-electrode cell was used for the electrochemical measurements. The working electrode was the test material with an immersed area of 1.0 cm^2. Platinum gauze and saturated calomel (SCE) electrodes were used as the counter and reference electrodes, respectively. Electrochemical testing was performed in naturally aerated 3.5 wt% NaCl solution with the pH = 5.8 at room temperature. Open circuit potential vs. time curves were measured for samples treated with different impact energies. Polarization curves were obtained at a scan rate of 0.2 mV/s, ranging from $-0.3\ V_{OCP}$ to $0.3\ V_{OCP}$. All electrochemical tests were performed under room temperature in a Faraday cage. To ensure the reproducibility of the results, experiments were repeated at least three times under the same experimental condition.

2.5. XRD, SEM and TEM

XRD patterns were performed using a Bruker D-8 Focus X-ray diffractometer with CuK_α radiation and at a 2θ scanning rate of 4°/min to determine the phase constituent in the surface layer. The cross-sectional

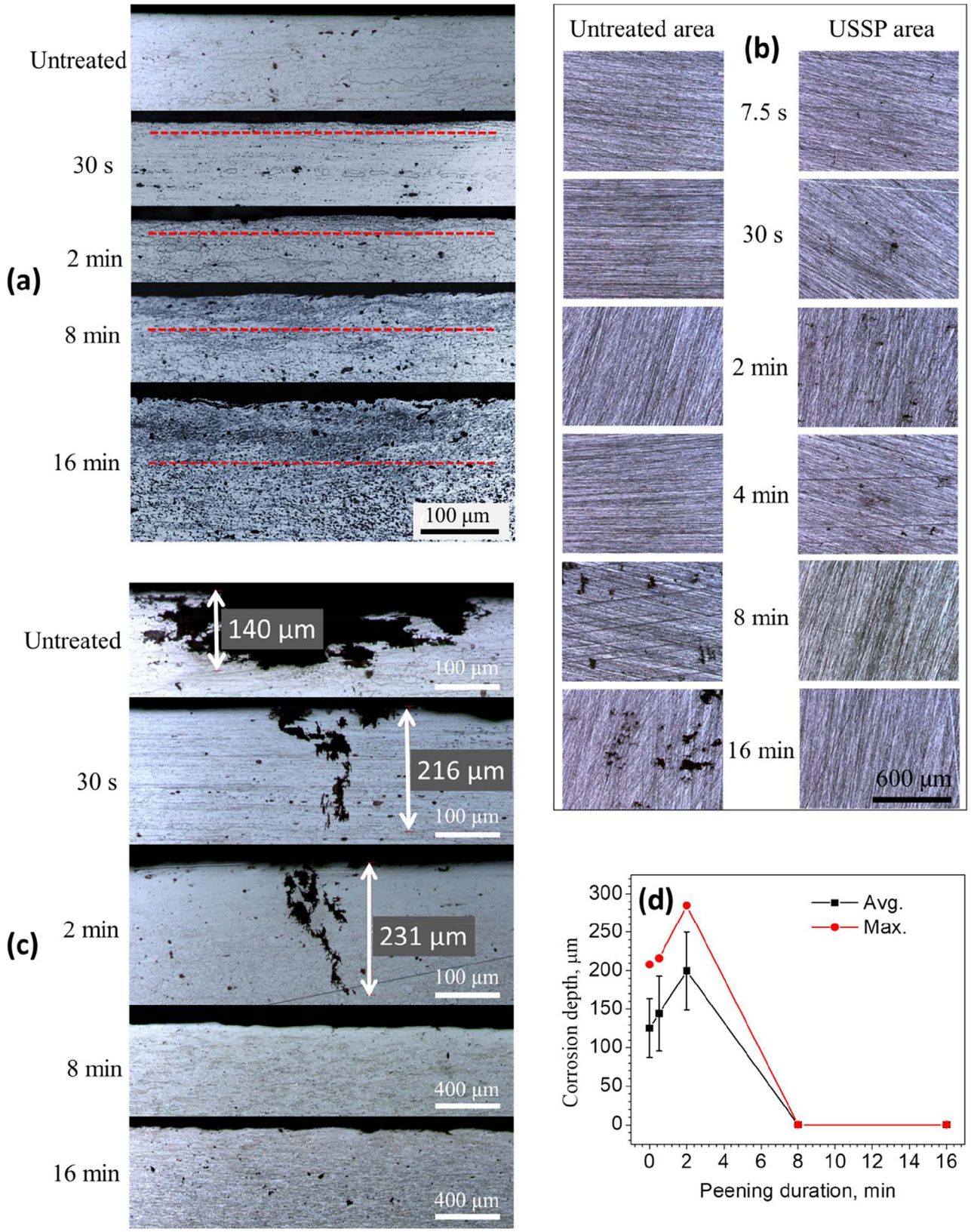

Fig. 4. (a) Cross-sectional optical microstructure of 3mm-8.2mm-80%-*t* group; (b) Surface morphologies showing the relative IGC depth of 3mm-8.2mm-80%-*t* group as compared with untreated sample; (c) Representative cross-sectional images of 3mm-8.2mm-80%-*t* group after IGC test; (d) The average and maximum corrosion depths of USSPed AA 7150 as a function of peening duration. Note that average corrosion depth is the average value of maximum depths of at least 15 images (each image is 2.679 mm in length and has a maximum depth). Maximum corrosion depth is the maximum depth of all the obtained images.

peened specimens were characterized by Phenom Desktop scanning electron microscopy (SEM) with energy dispersive X-ray spectroscopy (EDS). The characterization of the finer details of the microstructure in the USSPed alloy was performed using a JEOL 2000FX transmission electron microscope operated at 200 kV. The specimens for TEM examination was prepared by the FIB lift-Out method using FIB/SEM Dual Beam FEI Nova 200 [41]. The bright-field TEM images as well as selected area diffraction patterns were taken to characterize the fine microstructure of USSPed 7150 Al alloy.

3. Results

3.1. Corrosion depth

3.1.1. Effect of peening duration

Fig. 4a shows the optical microstructure of 3mm-8.2mm-80%-*t* group (t = 30s, 2 min, 8 min and 16 min). The effect of peening time on optical microstructure can be observed. The USSP treated surface layer is darker than substrate due to increasing grain boundaries on the surface layer. The thickness of USSP affected area increased with the increasing of peening duration. For t = 30s, 2 min, 8 min and 16 min, the peened area thickness is ~5 μm, ~20 μm, ~60 μm and ~100 μm, respectively.

Compared with the untreated sample, the effect of peening time on relative localized corrosion depth of the USSPed AA7150 samples can be intuitively observed from Fig. 4b. Samples peened with 8 min and 16 min had shallower pits than the untreated sample. The result shows that USSP can be beneficial for localized corrosion performance. However, for samples peened with duration shorter than 4 min, the pits on the peened alloy were deeper implying the deleterious effect of the USSP.

The representative corrosion morphologies of peened AA7150 alloys treated with different durations are shown in Fig. 4c. The morphologies can be used to measure corrosion depth quantitatively. The statistics of corrosion depth as a function of peening duration is shown in Fig. 4d. For the 3mm-8.2mm-80%-*t* samples with $t \geq 8$ min, the localized corrosion is completely inhibited. However, for samples peened with lower energies ($t \leq 4$ min), the pits exhibited a higher penetration ability than that of the untreated. The corrosion depth of the untreated sample (125 ± 38 μm in average and 208 μm in maximum) was lower than the corrosion depth of t = 30 s sample (145 ± 48 μm in average and 216 μm in maximum) and t = 2 min sample (200 ± 50 μm in average and 285 μm in maximum). Furthermore, as seen in Fig. 4c, pit mouth of t = 30s/2 min samples was much narrower than that of the untreated. The result indicated that more constricted pits were forming on samples with short pending duration.

3.1.2. Effect of ultrasonic amplitude

The effect of ultrasonic amplitude on optical microstructure of USSPed AA7150 can be seen from Fig. 5a. The group was referred to as 4mm-10mm-*A*–8 min. The reference means the USSP treatments were applied using stainless steel balls with 4 mm diameter as peening media, with 10 mm peening distance, 8 min duration and various values of ultrasonic amplitude. As was the case with the peening duration, the thickness of the USSP affected area increased with the increase of ultrasonic amplitude. For A = 40%, 60%, 80% and 100%, the peened area thickness was ~10 μm, ~25 μm, ~80 μm and ~150 μm, respectively.

Relative localized corrosion depth of the USSPed AA7150 as compared to the untreated sample can be seen in Fig. 5b. For A = 60%, 80% and 100%, the USSPed showed shallower pits than those of the untreated. However, for samples peened with 30% and 40% amplitude, the pits on the peened alloy were deeper, resulting in a deleterious effect on localized corrosion. The representative corrosion morphologies of peened AA7150 alloys treated with different peening amplitudes are shown in Fig. 5c. The corresponding statistics of corrosion depth is shown in Fig. 5d. For $A \geq 60\%$, the localized corrosion is completely eliminated. However, for samples peened with relative low impact energy (A = 40%), deep and needle-like pits are found that exhibited a higher penetration ability than that of the untreated sample. The average and maximum corrosion depth of the untreated sample was 92 ± 51 μm and 188 μm respectively. The untreated sample was lower than that of the A = 40% sample that had 140 ± 88 μm on average and 296 μm for the maximum. Note that the radius of the pits for the untreated alloy was much larger than that of the peened alloy.

3.1.3. Effect of peening distance

The effect of the peening distance (3mm-*d*-80%–8 min group) on the relative corrosion depth compared to the untreated alloy is shown in Fig. 6. For the 3mm-*d*-80%–8 min group, a larger value of d means lower impact energy. For the treated alloy with $d \geq 12$ mm (low impact energy), the corrosion depth of the USSPed area was deeper than that of the untreated. The alloys treated with smaller peening distances (higher impact energy) showed that the corrosion depth of the untreated sample was deeper. Deep needle-like pits formed on the samples with $d \geq 12$ mm. However, localized corrosion was eliminated on the samples with $d \leq 9$ mm as can be seen from the cross-sectional images after IGC immersion (shown in Fig. S1).

3.1.4. Effect of peening media diameter

The effect of peening media diameter (*D*-10mm-80%–8 min group) on relative corrosion depth is shown in Fig. 7. For D = 1 mm the corrosion depth of the USSPed area was deeper. Similar to the above results, the radius of the pits on the untreated alloy were much larger than that of peened alloy. For D = 3 and 5 mm, which corresponds to higher impact energies, the corrosion depth of untreated area was deeper. Localized corrosion was actually eliminated for D = 3 and 5 mm, as indicated by cross-sectional corrosion morphologies shown in Fig. S2.

The result of the current section showed that the localized corrosion was eliminated for alloys subjected to high impact energy USSP treatments, while deep needle-like pits were found for alloys subjected to low impact energy USSP treatment. All parameters of the USSP can influence impact energy. According to the optical micrographs shown in Fig. 4a and Fig. 5a, the current work defined the high and low impact based on the affected USSP thickness. For affected thickness less than 20 μm, the alloy is subjected to low impact energy USSP. For affected thickness more than 20 μm, the alloy is subjected to high impact energy USSP.

3.2. Galvanic interaction

Open circuit potential (OCP)-time curves as a function of peening parameters are shown in Fig. 8. The OCP curves of the untreated AA 7150 are also shown for comparison. For the AA 7150 treated with high impact energy USSP, the surface layer acts as a sacrificial anode in relation to the alloy beneath it. Thus, the treated surface layer caused by high impact energy is a protective layer when localized corrosion propagates. Conversely, if the alloy is treated with low impact energy USSP, the surface layer will act as a cathode and accelerates the corrosion rate of the substrate alloy. Interesting to note is that for samples with the sacrificial surface layer, the corrosion depth is shallower than that of the untreated samples. Otherwise, the corrosion depth of the peened area is deeper. The result implies that the galvanic interaction plays an important role in localized corrosion of the peened alloys.

The OCP value of the peened alloy is quite complicated and controlled by multiple factors. Some of which include the Fe & Ti-rich surface contamination induced from USSP setup or stainless-steel balls [4,24,33,42], more passive oxide film [17,25,39,43,44] and surface composition change [4]. Surface segregation of Zn and Cu on peened AA 7150 surface layers has been reported by previous work [4] from the current author's research group. Actually, Zn and Cu homogenously segregate on the surface layer, as shown in Fig. 9a. Consequently, Al

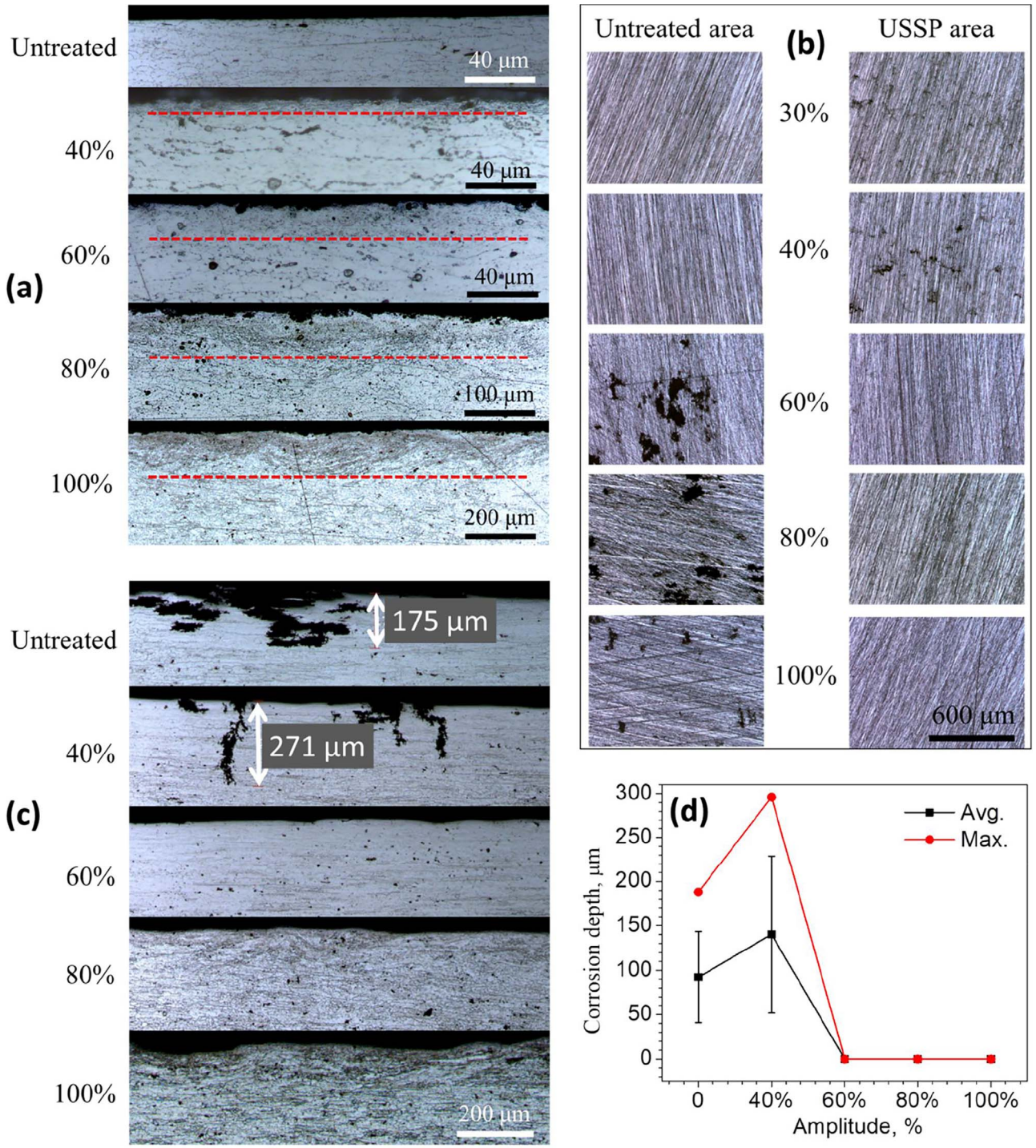

Fig. 5. (a) Cross-sectional optical microstructure of 4mm–10mm–*A*–8 min group; (b) Surface morphologies showing the relative corrosion depth of 4mm–10mm–*A*–8 min group as compared with the untreated sample; (c) Cross-sectional images of 4mm-10mm-*A*–8 min group after IGC test; (d) The average and maximum corrosion depths of USSPed AA 7150 as a function of ultrasonic amplitude. Note that average corrosion depth is the average value of maximum depths of at least 15 images (each image is 2.679 mm in length and has a maximum depth). Maximum corrosion depth is the maximum depth of all the obtained images.

and Mg compositions decline on the surface layer. The depletion of Mg may be due to the fact that the Mg has a negative value of solute-vacancy binding energy [45]. Surface segregation of peened AA 7150 is believed to be caused by the diffusion of alloying elements from sub-surface to surface layer along nano/sub-grain boundaries and dislocations. The driving force and kinetics of diffusion along grain/sub-grain boundaries and dislocations is out of the scope of this work and will be addressed with more details in the near future.

The schematic diagrams of OCP-composition relationship under solution with pH = 5.8 are shown in Fig. 9b and c. With a pH = 5.8, the enrichment of Zn in Al matrix would lead to the negative shifting of OCP. For low impact energy samples, Zn enrichment could not offset the effects of Cu enrichment, Mg depletion, surface contamination (Fe, Ti) and more passive oxide films. As a result, the OCP of the low energy peened alloy was more anodic than that of the untreated. During immersion into standard IGC solution, Fe & Ti-rich surface contamination layers exfoliate rapidly [4]. Thus, after the exfoliation of the Fe & Ti-rich layer, OCP of low energy peened samples probably would shift to

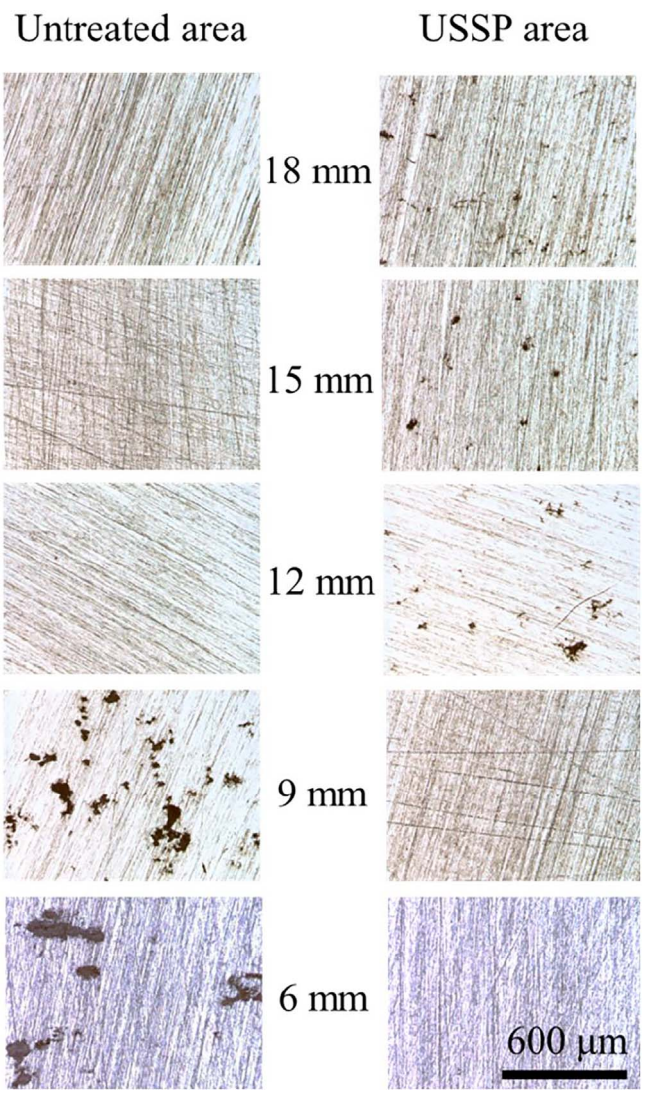

Fig. 6. Surfaces of 3mm-*d*-80%–8 min group after IGC test, which were used to compare the relative corrosion depth of USSP treated area and untreated area. By carefully grinding peened samples until the absence of pits on either USSP treated area or untreated area, the relative corrosion depth can be distinguished. From these images it can be seen that for treated alloy with $d \geq 12$ mm, the corrosion depth of USSPed area is deeper, while for samples with $d \leq 9$ mm the corrosion depth of untreated area is deeper.

the more cathodic direction and the surface layer turns to a protective layer. For high impact energy samples, Zn enrichment effect is more significant which can suppress the effects of Cu enrichment, Mg depletion, surface contamination and more passive oxide films. Therefore, OCP of high energy peened alloys are more cathodic than that of the controlled sample.

3.3. XRD and fine microstructure

Fig. 10a show the XRD patterns of the untreated, low energy peened (3mm-18mm-80%–8 min) and high energy peened (4mm-10mm-80%–8 min) AA 7150 along with the calculated Al ICDD PDF number 85–1327 [46]. The untreated sample was a typical rolled aluminium alloy which has the preferential orientation (220). The calculated pattern represents the aluminium with random orientations. By comparing the relative intensities of XRD peaks of peened samples with the calculated data, both low energy and high energy peened alloys can be predicted to have nearly random grain orientation in the very topmost surface. Random orientations can be further confirmed by texture characterization (shown in Fig. S3).

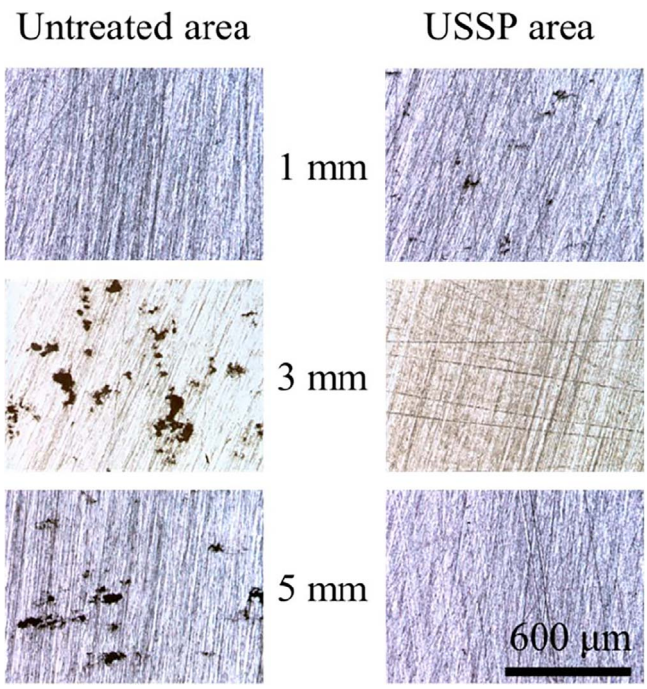

Fig. 7. Surfaces of *D*-10mm-80%–8 min group after IGC test, which were used to compare the relative corrosion depth of USSP treated area and untreated area. By carefully grinding peened samples until the absence of pits on either USSP treated area or untreated area, the relative corrosion depth can be distinguished. From these images it can be seen that for a treated alloy with $D = 1$ mm, the corrosion depth of USSPed area is deeper, while for samples with $D = 3, 5$ mm the corrosion depth of untreated area is deeper.

From Fig. 10b, the XRD peaks corresponding to η phases (pre-existing aging precipitations) disappear after USSP treatment indicating that η phases re-dissolve into Al matrix after USSP treatment. The result is due to the fact that USSP can extend solid solubility of alloying elements in the Al matrix. The re-dissolving of the η phases have been reported on the AA 7150 [47] and AA 7055 [48] subjected to grinding and AA 7075 [27] subjected to USSP. The homogenization of surface layer microstructure is expected to enhance localized corrosion resistance of the Al alloy. The disappearance of the XRD peaks for second phase particles also demonstrated that the segregated elements on the surface layer are in solid solution.

Peak broadening caused by microstrain and grain refinement can also be observed. The total broadening, β_{hkl}, is described by Eq. (1) [49] from which the values of mean microstrain and nanocrystalline grain size can be derived.

$$\beta_{hkl}{}^2 - \beta_0{}^2 = \left(\frac{K\lambda}{D_{hkl}\cos\theta}\right)^2 + (4\varepsilon\tan\theta)^2 \quad (1)$$

where K is a numerical factor frequently referred as the crystallite-shape factor ($K = 0.89$ for Al), λ the wavelength of incident wave, D_{hkl} the crystallite size in the direction perpendicular to the lattice planes, hkl the Miller indices of the planes being analysed, θ the Bragg angle, ε the microstrain and β_0 the instrumental broadening. β_{hkl} (full width at half maximum) was determined using Jade software (MDI JADE 7 Materials Data XRD Pattern Processing, Identification, and Quantification). The values of $\{\beta_{hkl}{}^2 - \beta_0{}^2\}$ as a function of bragg degree, 2θ, are shown in Fig. 10c and d for low energy peened and high energy peened AA 7150, respectively. By fitting the data using Eq. (1), the average grain size of low energy and high energy USSP treated AA 7150 was 39.87 ± 2.91 nm and 47.65 ± 6.04 nm, respectively. The mean microstrain of low energy and high energy peened AA 7150 is 0.25 ± 0.0065% and 0.25 ± 0.0089%, respectively.

Fig. 10e shows the shifting of the XRD peaks for the alloys after the USSP treatments. For both low energy and high energy peened alloys,

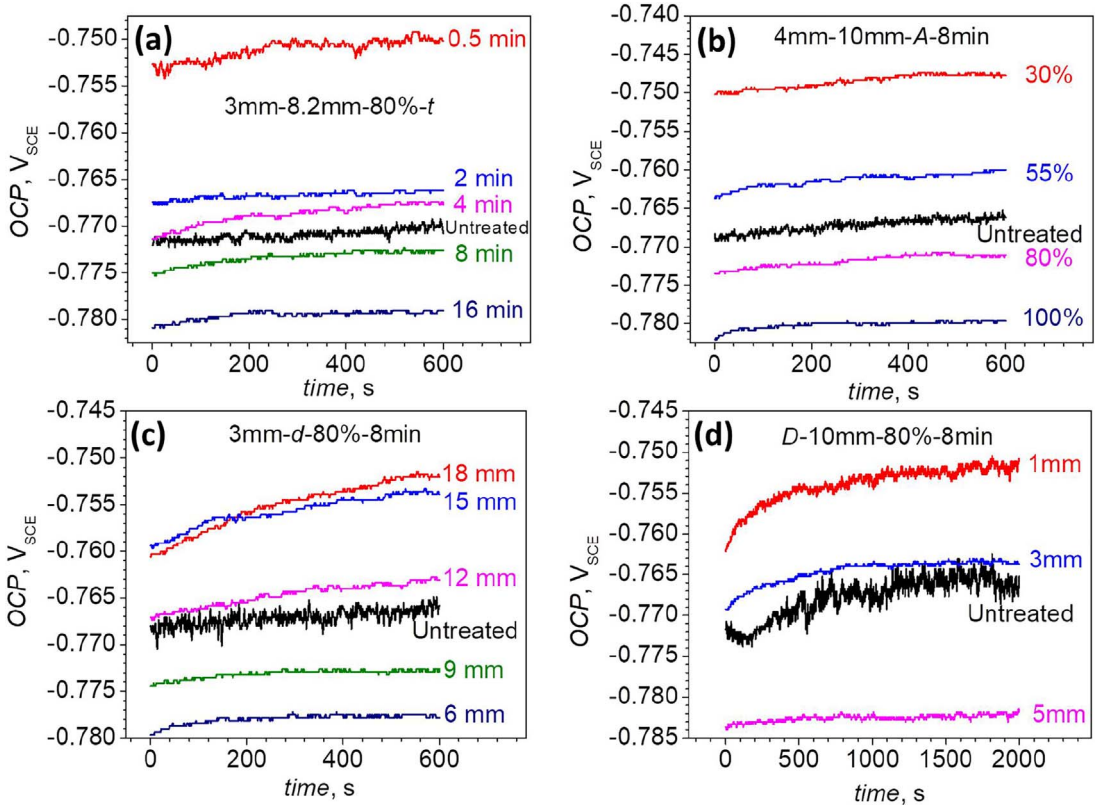

Fig. 8. Open circuit potential-time curves of AA 7150 in naturally aerated 3.5 wt.% NaCl solution with pH = 5.8 under room temperature: (a) as a function of peening duration *t*; (b) as a function of peening amplitude *A*; (c) as a function of peening distance *d*; (d) as a function of stainless steel ball diameter *D*.

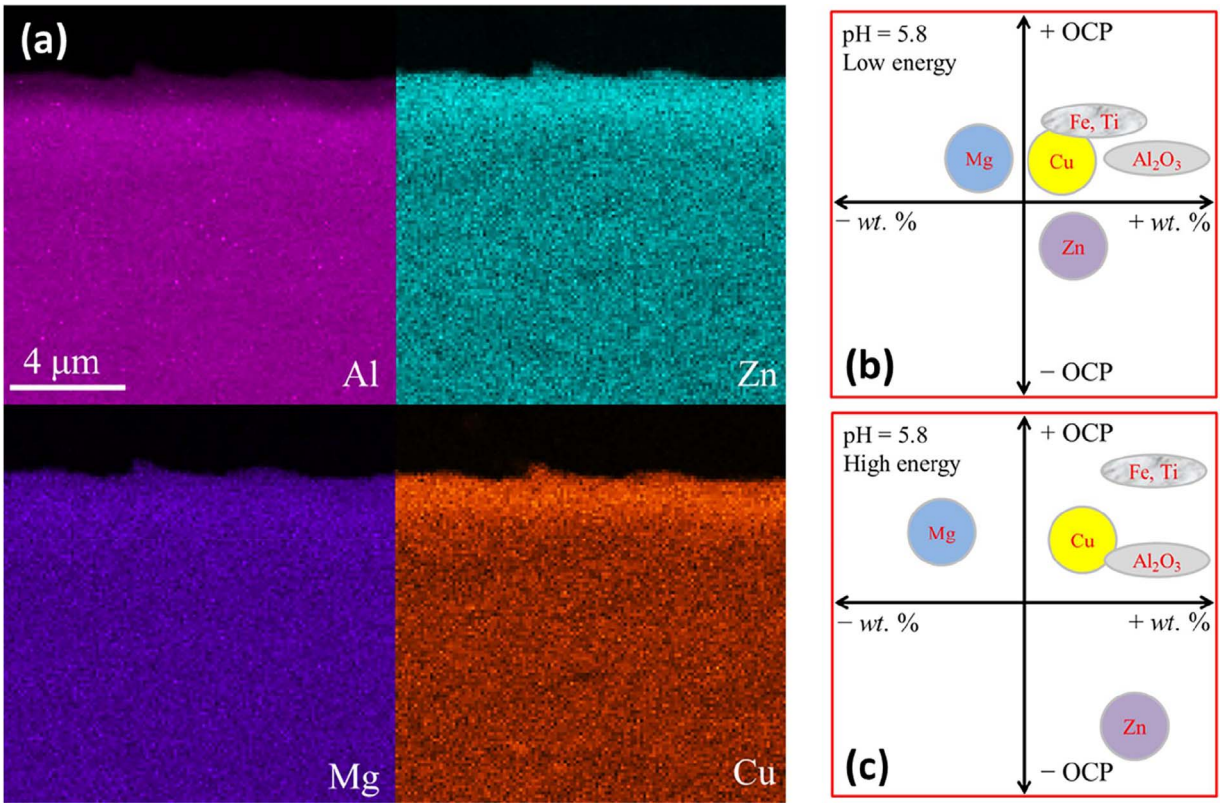

Fig. 9. (a) SEM-EDS mapping of cross-sectional image of 4mm-10mm-80%–16 min peened AA7150. Schematic diagrams of OCP-composition relationship under solution with pH = 5.8: (b) low impact energy treated AA7150; (c) high impact energy treated AA7150.

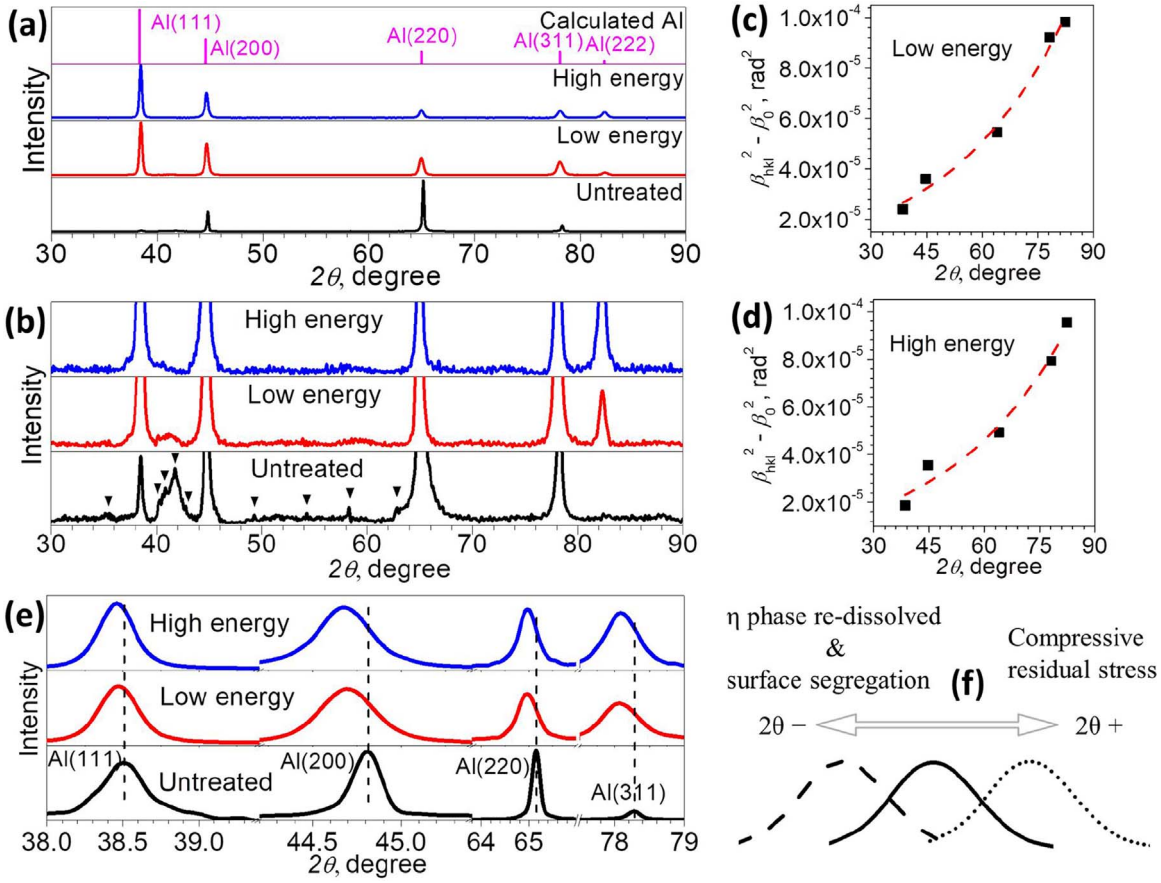

Fig. 10. (a) XRD patterns of the untreated, low energy peened, high energy peened AA 7150 and calculated Al; (b) XRD peaks of the untreated, low energy peened and high energy peened AA 7150 showing that second phase particles (η phases) dissolved into Al matrix after USSP; (c) The values of $\{\beta_{hkl}^2 - \beta_0^2\}$ as a function of Bragg degree 2θ for low energy peened (c) and high energy peened (d) AA 7150; (e) Shifting of peaks position after USSP, which showed that peaks shifted to the lower Bragg degree direction for both low and high energy peened alloys; (f) Schematic diagram showing how various factors influence the shifting of XRD peaks: peaks shift to the higher degree direction due to compressive residual stress caused by USSP; peaks shift to the lower degree direction due to re-dissolving of η phase and surface segregation.

peaks were found shifted to the lower Bragg degree direction. Both solid solution composition and residual stress status can influence the shifting of XRD peaks (Fig. 10f). The introduction of compressive residual stress after USSP is well documented [10,50], which results in the higher angle direction shifting of peaks due to the decrease of interplanar distance. Along those same lines, the increasing of the Zn and Cu solubility in Al (η phase dissolved and surface segregation) would increase interplanar distance resulting in the lower angle direction shifting of XRD peaks. As a result of those influences, the overall effect is lower angle direction shifting, indicating the effect of surface segregation suppressing the effect of compressive residual stress.

Cross-sectional SEM images of the untreated and 4mm–10mm–80%–8 min peened samples are shown in Fig. 11a and b, respectively. The original flattened grains are 10 ~ 30 μm in width. After shot peening, grain size reduces significantly. The closer to the surface the grains are the more refined they will be. TEM images of 4mm–10mm–80%–16 min USSPed AA 7150 are shown in Fig. 11c and d. The parallel lamellar-type nanobands (NBs) of elongated subgrains developed in the area ~10 μm to the topmost surface (Fig. 11c). Extended NBs are found to be 30–60 nm wide. Fig. 11d is a TEM micrograph illustrating the equiaxed microstructure in the nanometer regime (the area is ~5 μm to the top surface). Inset of Fig. 11c and d are ring-like diffraction patterns, indicating that there are many grains in the selected area of view. TEM results further confirm the disappearance of rolled texture as implied by XRD results. Additionally, TEM results show a good agreement with Wu's work [3] on AA 7075. Thus, gradient microstructure ranged from equiaxed nano-grains on surface layer to micro-grains in the interior alloy was achieved for AA 7150 using USSP treatment. The particular gradient microstructure accounts for the formation of needle-like pits with a narrow pit mouth.

4. Discussion

By manipulating ultrasonic shot peening parameters like peening duration, ultrasonic amplitude, peening distance and peening media diameter, USSP treated 7150 Al alloys with different impact energies were obtained. After immersion into standard IGC solution (57 g/L NaCl + 10 mL/L H_2O_2) under room temperature for 24 h, localized corrosion behaviour of USSPed samples with different impact energies are schematically summarized in Fig. 12. Deep needle-like pits, as shown in Fig. 12b, are observed on low energy peened samples (generally the thickness of affected zone ≤ 20 μm). The penetration depth of needle-like pits was deeper than that of the untreated sample (Fig. 12a), indicating better penetration ability. Moreover, the needle-like pits are characterized with a much narrower pit mouth (~ 20 μm) than that of the untreated sample (~ several hundred μm). For high energy peened samples (the thickness of affected zone > 20 μm), localized corrosion is surprisingly eliminated, as shown in Fig. 12c. The resulting phenomena will be discussed in two phases of pitting corrosion kinetics: pit initiation and pit propagation.

4.1. Pit initiation

Pitting potential, E_{pit}, is the lowest potential from which pitting initiation is possible on a passive metal (CEN/TC262/WG1 N16 definition). It characterizes the metal's resistance to pit initiation. Tafel

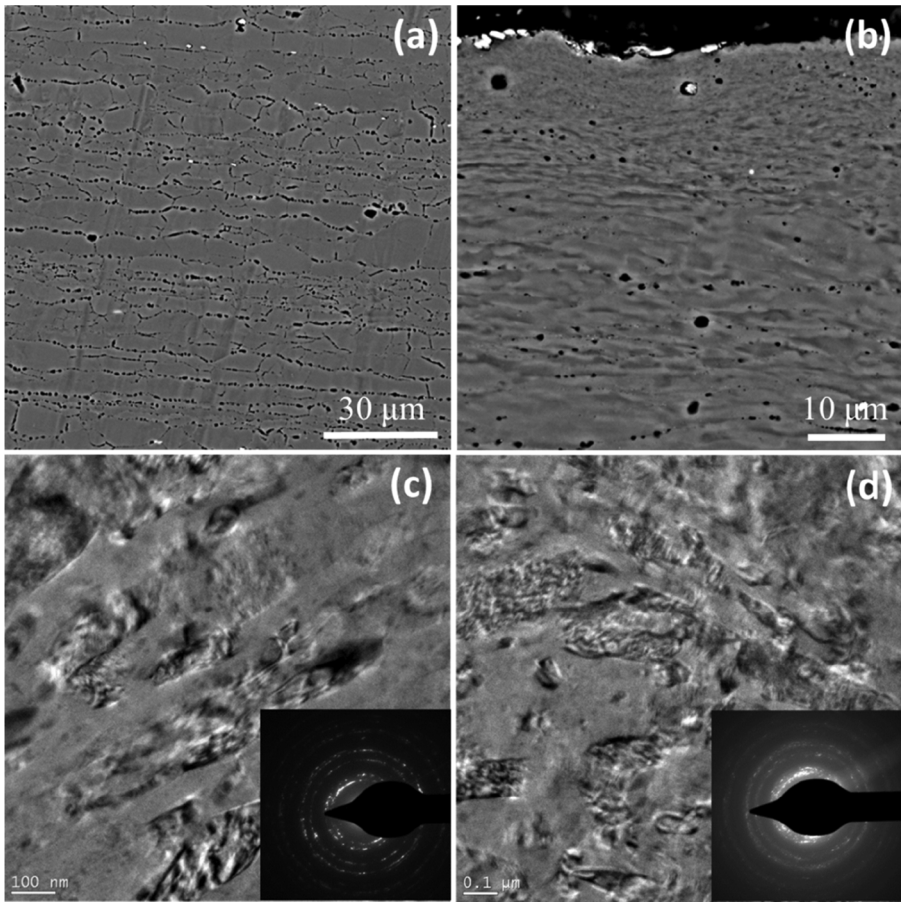

Fig. 11. Cross-sectional SEM images of the untreated (a) and 4mm-10mm-80%–8 min USSPed AA 7150 (b). The bright field TEM observation showing nano-sized grains of 4mm-10mm-80%–16 min peened AA7150 and the diffraction pattern of the corresponded area: (c) ~10 μm to the top surface; (d) ~5 μm to the top surface.

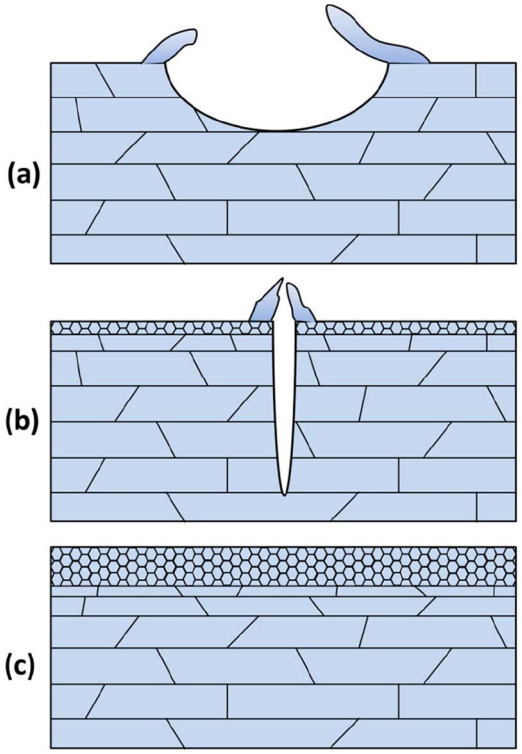

Fig. 12. Schematic diagrams of pit morphologies for 7150 aluminium alloys without (a), with low impact energy (b) and high impact energy (c) USSP treatment after immersed into standard IGC solution for 24 h.

plots of the untreated and USSPed AA7150 (3mm-18mm-80%–16 min) are shown in Fig. 13a. Because when the oxide film ruptures the corrosion current would increase significantly, E_{pit} is determined as the potential at which the corresponding current increases sharply from the passive current level. After USSP (3mm-18mm-80%–16 min) treatment, E_{pit} value of alloy increases from -0.771 ± 0.008 to -0.723 ± 0.007 V_{SCE}. In addition, it can be also seen from Fig. 13a that the studied alloy after USSP treatment shows better passivation ability than that of the untreated. Actually, E_{pit} shifts to the more anodic direction with increasing peening duration (t ranges from 30 s to 16 min for 3mm-18mm-80%-*t* group), as depicted by Fig. 13b. To ensure the reproducibility of E_{pit} results, Tafel plots were repeated at least three times under the same experimental condition.

The corrosion rate of USSPed sample was higher than that of the untreated sample, as can be easily seen from Fig. 13a. The result was due to surface contamination effect, which has been systematically studied in our previous work [4]. Polarization results indicate that USSP surface layer with nano-sized grains can retard and postpone the initiation of pitting corrosion. The retardation is mainly due to grain refinement, distortion effect, and homogenization of the microstructure on the surface layer caused by USSP, as indicated by XRD and TEM results. Compressive residual layers also account for the pitting initiation resistance improvement, as indicated by Liu's work [10]. However, for the 3mm-18mm-80%-*t* (t up to 16 min) group, all specimens are characterized by a greater corrosion depth than the untreated counterpart. The reason behind this is because the peening distance, 18 mm, is too large to employ high impact energy on the alloy surface. The final localized corrosion depth depends on both initiation and propagation kinetics of pitting process. Unlike improving pit initiation resistance, the propagation rate of pits is accelerated as a result of the gradient microstructure caused by USSP.

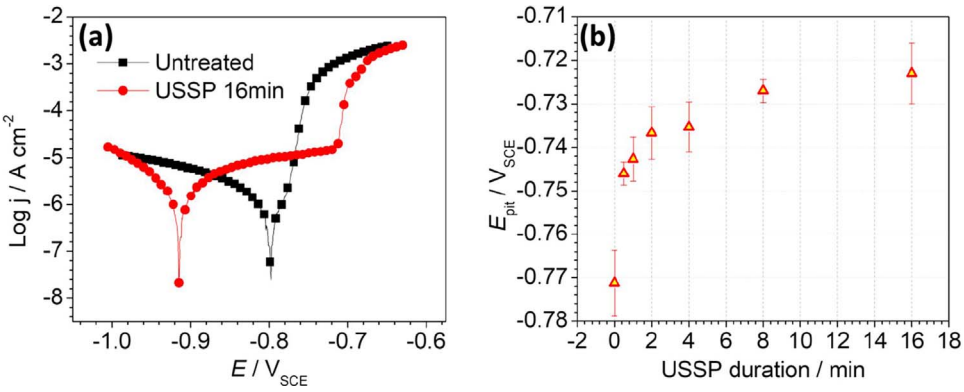

Fig. 13. (a) Tafel plots of the untreated and 3mm-18mm-80%–16 min peened AA 7150 in naturally aerated 3.5 wt.% NaCl solution with pH = 5.8 under room temperature; (b) pitting potential E_{pit} as a function of peening duration (3mm-18mm-80%-t group). For each condition the value of E_{pit} was determined using at least three parallel experiments.

4.2. Pit propagation

A 10-step mechanism of aluminium pitting with more details is displayed below [51].

1. The Cl^- adsorption in microflaws of the oxide film, assisted by the high electric field.
2. Slow oxygen reduction on the cathodic area, charging the double-layer capacitance (~50 μF/cm^2)
3. Dielectric breakdown of the oxide film at weak points corresponding to the microflaws
4. Fast aluminium oxidation of bare aluminium producing soluble chloride and oxychloride complexes at the bottom of flaws.
5. Dissolution of chloride complexes and repassivation of pits. These first five steps produce 10^6/cm^2 micropits of size 0.1–1 μm.
6. For some different (often unexplained) reasons, a few micropits propagate. The unexplained propagation requires the stabilization of a chloride/oxychloride layer at the active bottom of pits. The layer should be renewed faster than it dissolves, which implies a large enough cathodic area, resulting from the repassivation of the surrounding competitive pits, formed during step 4.
7. Hydrolysis of soluble chlorides/oxychlorides, resulting in the acidification (to pH 3) of the solution within the pits.
8. Hydroxide dissolution inside pits and precipitation of aluminium hydroxide outside pits resulting in the formation of cone-shaped or chimney-shaped accumulations of corrosion products at the mouths of pits, which limits solution exchange with the bulk solution.
9. Aluminium auto-corrosion inside the pits due to the aggressive hydrochloric acid solution, producing H_2 bubbles, which limits Cl^- build up and acidification inside the propagating pits.
10. Repassivation and pit death when I_{pit}/r_{pit} (r is the radius of the pit) decreases to 10^{-2} A/cm [52]. The chloride/oxychloride film is dissolved and replaced by a passive oxide film. The solution within the pit is diluted and will revert to the composition of the bulk solution.

As suggested by step 6 and 7, a concentrated $AlCl_3$ solution with pH = 3 forms inside the pit. The stabilization of the propagating pits requires a critical Cl^- and H^+ concentration to prevent pit repassivation. A propagating pit will continue to grow as long as the micro-galvanic cell can renew the solution within the pit more rapidly than diffusion and hydrogen bubbles tend to dilute said pit. Compared with the untreated alloy, the pit mouth of the low energy peened sample is much narrower and the corrosion product “chimney” is easier to form (Fig. 12b). In other words, the pit of the low energy peened alloy is much more constricted than that of the untreated sample. Therefore, the diffusion of Cl^- from inside of the pit to the bulk solution can be suppressed which helps meet the critical Cl^- inside the pit. The much narrower pit mouth is a result of exfoliation of equiaxed nano/ultrafine grains. While for the untreated alloy, the wide open pit mouth helps the homogenization of the pit solution with the bulk solution, which results in pit death. Wide open-mouth pits forming on the untreated sample is due to the exfoliation of large flattened grains during the corrosion process. From step 10 we also know that pits with a smaller radius are more difficult to repassivate and will continue to penetrate the alloy [52]. The radius of pits on the low impact energy peened alloy is much smaller than that of the untreated sample. As a result, pits of the low energy peened alloy continue to grow, which results in a deeper corrosion depth.

No obvious pits are observed on the high energy peened AA 7150 after 24 h immersion in standard IGC solution. The reason is that after 24 h immersion in standard IGC solution, pits have not yet initiated or have initiated but haven’t yet penetrated the topmost surface layer with nano/ultrafine grains. By increasing the aggressivity of the solution or prolonging the immersion time, the author found that even for the high energy peened alloy the USSP surface layer is penetrated. Fig. 14 shows representative cross-sectional images of untreated (a) and a high energy (4mm-10mm-100%–8 min) peened sample (b) after 72 h immersed into

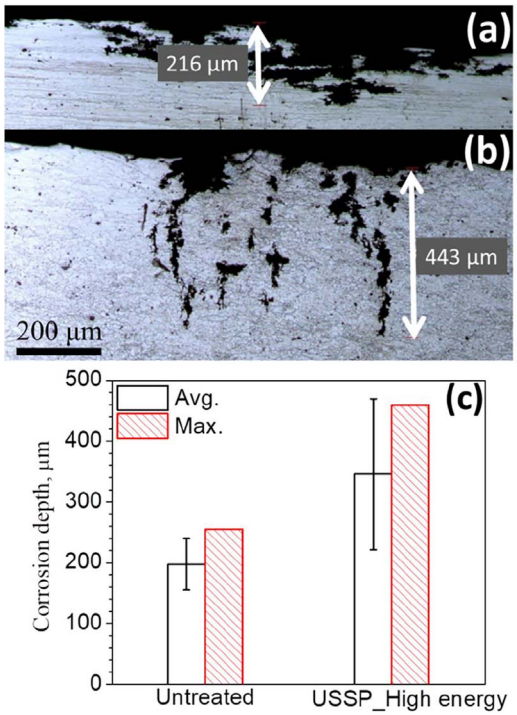

Fig. 14. Representative cross-sectional images of the untreated (a) and high impact energy (4mm-10mm-100%–8 min) peened sample (b) after 72 h immersed into standard IGC solution under room temperature; the solution was refreshed every 24 h. (c) Statistics of corrosion depth after 72 h immersion for the untreated and 4mm-10mm-100%–8 min peened sample.

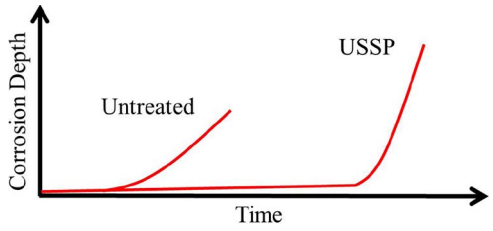

Fig. 15. Pit initiation and propagation kinetics of the untreated and USSP treated AA 7150.

standard IGC solution under room temperature (solution was refreshed every 24 h). The corresponding corrosion depth statistics is shown in Fig. 14c. As can be seen in the figure, corrosion depth of high energy peened alloy is as deep as 400 μm, indicating that pits already penetrated the USSP affected ~150 μm thick layer. As expected, once initiated or penetrated through the topmost ultrafine layer, the pit propagates rapidly and a deeper corrosion depth is observed. Similar results (not shown) also are found for high energy peened alloys after immersion into a more aggressive solution (28.5 g NaCl + 10 mL 37% HCl + 1 L H_2O).

In a given corrosion environment, for both low energy or high energy peened AA 7150 samples, pits first initiate and then continue to propagate down to the substrate alloy. Therefore, the authors propose a more general model of localized corrosion kinetics for the 7150 aluminium alloys with and without USSP treatment, which is schematically shown in Fig. 15. In the first stage, USSP significantly enhances the localized corrosion initiation resistance of AA7150. The phenomenon is mainly due to the formation of nano/ultrafine grains layer on the surface of peened alloy, the homogenization of microstructure and the compressive residual stress effect. These factors can retard and postpone the process of localized corrosion initiation. The higher impact energy is the longer the induction period will be. In the second stage, after being initiated, the pit's propagation rate is accelerated by a gradient microstructure. The acceleration is because of the exfoliation of nano/ultrafine grains which results in a much narrower pit mouth and more constricted pit morphology. Penetration rate is accelerated by limiting diffusion between the inside of the pit and bulk solution.

The localized corrosion performance of USSPed AA 7150 is a comprehensive result of pit initiation and propagation kinetics. The two phases of pitting are strongly dependent on immersion time, solution aggressivity and the thickness of nano/ultrafine grains layer influenced by impact energy. The accelerated corrosion propagation kinetics seems to limit the application of SMAT/USSP technologies. Nonetheless, under many practical service environments of aluminium alloys, as long as proper processing parameters are selected, USSP can still find great potential in application due to its significant corrosion initiation retarding ability. According to Fig. 15, materials with novel microstructure can be designed to further extend the induction period and decrease the propagation rate, achieving better corrosion resistance and sustainability.

5. Conclusions

As revealed by SEM-EDS, XRD and TEM, surface nanocrystallization, surface segregation and the dissolving of η phases were found on the surface layer of USSPed AA 7150. The relationship between gradient microstructure and localized corrosion kinetics of AA 7150 was constructed.

USSP significantly enhances pits initiation resistance but accelerates pits propagation kinetics of AA 7150. The enhancement of pits initiation resistance was due to nano/ultrafine grains layer on the surface of peened alloy, the homogenization of the microstructure, and the compressive residual stress effect caused by USSP. The accelerated propagation kinetics were the result of constricted pit morphology caused by a gradient microstructure. The result limits the diffusion with the bulk solution and decreases the pit's repassivation ability. In conclusion, localized corrosion behaviour of USSPed AA 7150 is a comprehensive result of pit initiation and propagation kinetics, which depends on immersion time, solution aggressivity and the thickness of nano/ultrafine-grain layer influenced by impact energy.

Acknowledgments

The current work was supported by the Center for Technology Development at Purdue University. The financial support of the China Scholarship Council is also gratefully acknowledged. The authors would like to thank Prof. Xiaoming Wang and Mr. Xingtao Liu for their assistance on TEM work. Mr. Ian McAdams is highly acknowledged for his corrections on English. The current paper is dedicated to my dear mentor Prof. Qiyuan Chen, who unfortunately passed away in March, 2016. His guidance and wisdom will be forever remembered.

References

[1] N. Tao, Z. Wang, W. Tong, M. Sui, J. Lu, K. Lu, An investigation of surface nanocrystallization mechanism in Fe induced by surface mechanical attrition treatment, Acta Mater. 50 (2002) 4603–4616.
[2] W. Tong, N. Tao, Z. Wang, J. Lu, K. Lu, Nitriding iron at lower temperatures, Science 299 (2003) 686–688.
[3] X. Wu, N. Tao, Y. Hong, B. Xu, J. Lu, K. Lu, Microstructure and evolution of mechanically-induced ultrafine grain in surface layer of AL-alloy subjected to USSP, Acta Mater. 50 (2002) 2075–2084.
[4] Q. Sun, Q. Han, X. Liu, W. Xu, J. Li, The effect of surface contamination on corrosion performance of ultrasonic shot peened 7150 Al alloy, Surf. Coat. Technol. 328 (2017) 469–479.
[5] X. Li, K. Lu, Playing with defects in metals, Nat. Mater. 16 (2017) 700–701.
[6] Y. Estrin, A. Vinogradov, Extreme grain refinement by severe plastic deformation: a wealth of challenging science, Acta Mater. 61 (2013) 782–817.
[7] T. Roland, D. Retraint, K. Lu, J. Lu, Fatigue life improvement through surface nanostructuring of stainless steel by means of surface mechanical attrition treatment, Scripta Mater. 54 (2006) 1949–1954.
[8] Y. Zhang, Z. Han, K. Wang, K. Lu, Friction and wear behaviors of nanocrystalline surface layer of pure copper, Wear 260 (2006) 942–948.
[9] Z. Wang, N. Tao, W. Tong, J. Lu, K. Lu, Diffusion of chromium in nanocrystalline iron produced by means of surface mechanical attrition treatment, Acta Mater. 51 (2003) 4319–4329.
[10] X. Liu, G. Frankel, Effects of compressive stress on localized corrosion in AA2024-T3, Corros. Sci. 48 (2006) 3309–3329.
[11] Z. Ye, D. Liu, C. Li, X. Zhang, Z. Yang, M. Lei, Effect of shot peening and plasma electrolytic oxidation on the intergranular corrosion behavior of 7A85 aluminum alloy, Acta Metall. Sin. (English Lett.) 27 (2014) 705–713.
[12] M. Abdulstaar, M. Mhaede, M. Wollmann, L. Wagner, Investigating the effects of bulk and surface severe plastic deformation on the fatigue, corrosion behaviour and corrosion fatigue of AA5083, Surf. Coat. Technol. 254 (2014) 244–251.
[13] R. Waikar, Y. Guo, J. Liu, Z. Liu, Electrochemical corrosion behavior of surface nanocrystallized steel and aluminum alloys by air blast shot peening (ABSP), Flexible Automation (ISFA), International Symposium on IEEE (2016) 359–365.
[14] M. Navaser, M. Atapour, Effect of friction stir processing on pitting corrosion and intergranular attack of 7075 aluminum alloy, J. Mater. Sci. Technol. 33 (2016) 155–165.
[15] S. Jelliti, C. Richard, D. Retraint, T. Roland, M. Chemkhi, C. Demangel, Effect of surface nanocrystallization on the corrosion behavior of Ti–6Al–4 V titanium alloy, Surf. Coat. Technol. 224 (2013) 82–87.
[16] C. Zhang, W. Song, F. Li, X. Zhao, Y. Wang, G. Xiao, Microstructure and corrosion properties of Ti-6Al-4 V alloy by ultrasonic shot peening, Int. J. Electrochem. Sci. 10 (2015) 9167–9178.
[17] S. Kumar, K. Chattopadhyay, V. Singh, Effect of surface nanostructuring on corrosion behavior of Ti–6Al–4 V alloy, Mater. Charact. 121 (2016) 23–30.
[18] A.A. Ahmed, M. Mhaede, M. Wollmann, L. Wagner, Effect of micro shot peening on the mechanical properties and corrosion behavior of two microstructure Ti–6Al–4 V alloy, Appl. Surf. Sci. 363 (2016) 50–58.
[19] T. Balusamy, T.S. Narayanan, K. Ravichandran, I.S. Park, M.H. Lee, Influence of surface mechanical attrition treatment (SMAT) on the corrosion behaviour of AISI 304 stainless steel, Corros. Sci. 74 (2013) 332–344.
[20] P. Chui, K. Sun, C. Sun, X. Yang, T. Shan, Effect of surface nanocrystallization induced by fast multiple rotation rolling on hardness and corrosion behavior of 316L stainless steel, Appl. Surf. Sci. 257 (2011) 6787–6791.
[21] M. Ilieva, R. Radev, Effect of severe plastic deformation by ECAP on corrosion behaviour of aluminium alloy AA 7075, Arch. Mater. Sci. 56 (2016) 56.
[22] N. Li, S. Shi, J. Luo, J. Lu, N. Wang, Effects of surface nanocrystallization on the corrosion behaviors of 316L and alloy 690, Surf. Coat. Technol. 309 (2017) 227–231.
[23] D. Asquith, A. Yerokhin, J. Yates, A. Matthews, The effect of combined shot-peening and PEO treatment on the corrosion performance of 2024 Al alloy, Thin Solid Films

516 (2007) 417–421.
[24] L. Wen, Y. Wang, Y. Zhou, L. Guo, J. Ouyang, Iron-rich layer introduced by SMAT and its effect on corrosion resistance and wear behavior of 2024 Al alloy, Mater. Chem. Phys. 126 (2011) 301–309.
[25] U. Trdan, J. Grum, Evaluation of corrosion resistance of AA6082-T651 aluminium alloy after laser shock peening by means of cyclic polarisation and ElS methods, Corros. Sci. 59 (2012) 324–333.
[26] U. Zupanc, J. Grum, Effect of pitting corrosion on fatigue performance of shot-peened aluminium alloy 7075-T651, J. Mater. Process. Technol. 210 (2010) 1197–1202.
[27] V. Pandey, J. Singh, K. Chattopadhyay, N.S. Srinivas, V. Singh, Influence of ultrasonic shot peening on corrosion behavior of 7075 aluminum alloy, J. Alloys Compd. 723 (2017) 826–840.
[28] T. Balusamy, S. Kumar, T.S. Narayanan, Effect of surface nanocrystallization on the corrosion behaviour of AISI 409 stainless steel, Corros. Sci. 52 (2010) 3826–3834.
[29] R. Gupta, B. Sunil Kumar, R. Sundar, P. Ram Sankar, P. Ganesh, R. Kaul, V. Kain, K. Ranganathan, K. Bindra, B. Singh, Enhancement of intergranular corrosion resistance of type 304 stainless steel through laser shock peening, Corros. Eng. Sci. Technol. (2017) 1–6.
[30] W. Friske, J. Page, Shot peening to prevent the corrosion cracking of austenitic stainless steels, J. Mater. Energy Syst. 1 (1979) 20–32.
[31] W. Tomlinson, S. Matthews, Shot peening and the intergranular corrosion of sensitized welds in type 430 stainless steel, J. Mater. Sci. Lett. 7 (1988) 493–494.
[32] E. Lemaire, Y. Le Guernic, F. Roch, C. Scott, Shot peening to prevent intergranular corrosion of ferritic stainless steel, Proc. Int. Conf. on Shot Peening (ICSP-6), San Francisco, CA, 1996.
[33] D. Fabijanic, A. Taylor, K. Ralston, M.-X. Zhang, N. Birbilis, Influence of surface mechanical attrition treatment attrition media on the surface contamination and corrosion of magnesium, Corrosion 69 (2012) 527–535.
[34] P. Jiang, Q. Wei, Y. Hong, J. Lu, X. Wu, In situ synthesis of nanocrystalline intermetallic layer during surface plastic deformation of zirconium, Surf. Coat. Technol. 202 (2007) 583–589.
[35] Y. Kameyama, J. Komotori, Effect of micro ploughing during fine particle peening process on the microstructure of metallic materials, J. Mater. Process. Technol. 209 (2009) 6146–6155.
[36] Y. Kameyama, J. Komotori, Tribological properties of structural steel modified by fine particle bombardment (FPB) and diamond-like carbon hybrid surface treatment, Wear 263 (2007) 1354–1363.
[37] M. Vasylyev, B. Mordyuk, S. Sidorenko, S. Voloshko, A. Burmak, Corrosionof 2024 alloy after ultrasonic impact cladding with iron, Surf. Eng. (2017) 1–6.
[38] K. Lu, J. Lu, Nanostructured surface layer on metallic materials induced by surface mechanical attrition treatment, Mater. Sci. Eng. A 375 (2004) 38–45.
[39] R. Huang, Y. Han, The effect of SMAT-induced grain refinement and dislocations on the corrosion behavior of Ti–25Nb–3Mo–3Zr–2Sn alloy, Mater. Sci. Eng. C 33 (2013) 2353–2359.
[40] M. Rakita, M. Wang, Q. Han, Y. Liu, F. Yin, Ultrasonic shot peening, Int. J. Comput. Mater. Sci. Surf. Eng. 5 (2013) 189–209.
[41] L.A. Giannuzzi, J.L. Drown, S.R. Brown, R.B. Irwin, F.A. Stevie, Applications of the FIB lift-out technique for TEM specimen preparation, Microsc. Res. Tech. 41 (1998) 285–290.
[42] L. Wen, Y. Wang, Y. Jin, X. Ren, Comparison of corrosion behaviour of nanocrystalline 2024-T4 Al alloy processed by surface mechanical attrition treatment with two different mediums, Corros. Eng. Sci. Technol. 50 (2015) 425–432.
[43] U. Trdan, J. Grum, SEM/EDS characterization of laser shock peening effect on localized corrosion of Al alloy in a near natural chloride environment, Corros. Sci. 82 (2014) 328–338.
[44] R. Gupta, D. Fabijanic, R. Zhang, N. Birbilis, Corrosion behaviour and hardness of in situ consolidated nanostructured Al and Al–Cr alloys produced via high-energy ball milling, Corros. Sci. 98 (2015) 643–650.
[45] C. Wolverton, Solute–vacancy binding in aluminum, Acta Mater. 55 (2007) 5867–5872.
[46] H.E. Swanson, E. Tatge, R.K. Fuyat, Standard X-ray Diffraction Powder Patterns, (1953).
[47] B. Liu, X. Zhang, X. Zhou, T. Hashimoto, J. Wang, The corrosion behaviour of machined AA7150-T651 aluminium alloy, Corros. Sci. 126 (2017) 265–271.
[48] S.-S. Wang, J.-T. Jiang, G.-H. Fan, A. Panindre, G. Frankel, L. Zhen, Accelerated precipitation and growth of phases in an Al-Zn-Mg-Cu alloy processed by surface abrasion, Acta Mater. 131 (2017) 233–245.
[49] B.E. Warren, X-ray Diffraction, Courier Corporation, 1969.
[50] M. Kobayashi, T. Matsui, Y. Murakami, Mechanism of creation of compressive residual stress by shot peening, Int. J. Fatigue 20 (1998) 351–357.
[51] M. Reboul, T. Warner, H. Mayer, B. Barouk, A ten step mechanism for the pitting corrosion of aluminium alloys, Corros. Rev. 15 (1997) 471–496.
[52] S. Pride, J. Scully, J. Hudson, Metastable pitting of aluminum and criteria for the transition to stable pit growth, J. Electrochem. Soc. 141 (1994) 3028–3040.